

Received: 2021.07.17

Accepted: 2021.10.11

Available online: 2021.10.27

Published: 2022.02.01

A Novel Predictive Model Incorporating Ferroptosis-Related Gene Signatures for Overall Survival in Patients with Lung Adenocarcinoma

Authors' Contribution:

Study Design A
Data Collection B
Statistical Analysis C
Data Interpretation D
Manuscript Preparation E
Literature Search F
Funds Collection G

ABE **Yuli Wang*** 
BC **Yanbin Pan***
AD **Jianchun Wu**
B **Yingbin Luo**
F **Zhihong Fang**
F **Rongzhong Xu**
DF **Wenjing Teng**
AF **Min Chen**
AG **Yan Li**

Department of Oncology, Shanghai Municipal Hospital of Traditional Chinese Medicine, Shanghai University of Traditional Chinese Medicine, Shanghai, PR China

* Yuli Wang and Yanbin Pan contributed equally to the manuscript

Corresponding Authors: Yan Li, e-mail: yan.xiaotian@shutcm.edu.cn, Min Chen, e-mail: 1923904859@qq.com

Financial support: This study was funded by the National Nature Science Foundation of China (81973795), 2017 Medical Guidance (Traditional Chinese and Western Medicine) Science and Technology Support Project of Shanghai Science and Technology Commission (17401933500), Shanghai Pujiang Program (2020PJD057), and Natural Science Foundation of Shanghai (19ZR1452200)

Conflict of interest: None declared

Background: Lung adenocarcinoma (LUAD) is the predominant histological type of lung cancer with high morbidity and mortality. Ferroptosis is regarded as a new pattern of programmed cell death concerned with the progression of lung cancer characterized by lipid peroxidation. Nevertheless, the prognostic role of ferroptosis-related genes for LUAD warrant to be explored.

Material/Methods: RNA sequencing and relevant clinical patient data were obtained from public-access databanks. A prognostic model was constructed through the LASSO Cox regression in the cancer genome atlas cohort. The diagnostic value of the prognostic model was further evaluated in the gene expression omnibus cohort.

Results: Most of the ferroptosis-related genes (69.9%) were differentially expressed between tumor and adjacent non-cancerous tissues. 43 differentially expressed genes showed a close association with the prognosis of LUAD patients (adjusted p -value <0.05). An 18-gene signature was built and applied to assign patients into high vs low-risk groups. Compared with the high-risk group, patients defined as the low-risk group suffered significantly prolonged OS. Both uni- and multivariate analyses demonstrated that the signature-based score served as a crucial role in influencing the OS of LUAD patients (hazard ratio >1 , $p < 0.001$). The immunity-related signaling pathway was enriched in the functional analysis and the infiltration of the immune cells showed a great difference between groups.

Conclusions: The predictive model could be applied for prognostic prediction for LUAD. Targeting ferroptosis could be a possible curative strategy against LUAD, and immunomodulation may be one of the potential mechanisms.

Keywords: **Ferroptosis • Lung Neoplasms • Survival • Transcriptome**

Full-text PDF: <https://www.medscimonit.com/abstract/index/idArt/934050>

 3916

 2

 11

 54



Background

At present, lung cancer is constantly threatening public health worldwide for its high incidence and mortality [1,2]. Among them, lung adenocarcinoma (LUAD) is the majority commonly diagnosed histological subtype [3]. Despite the substantial advances in targeted molecular therapy and immunotherapy, the overall 5-year survival benefit is still limited, only about 18% in China [4]. So, what is the major cause of the low survival rate for LUAD patients?

In our opinion, on the one hand, for most LUAD patients with early-stage disease who undergo surgery, a lack of specific prognostic biomarkers is the main factor that restricts post-operative monitoring. On the other hand, although several mutation driver genes such as epidermal growth factor receptor gene mutations, ROS1 rearrangements, etc. have now been elucidated. Nevertheless, there is still a large proportion of LUAD patients who cannot benefit from current targeted therapies for the lack of novel effective targets [5]. Therefore, it is of great benefit to identify novel biomarkers with pathological and prognostic significance, not only for the risk assessment of LUAD patients' prognosis but also for the development of therapeutic targets for LUAD.

Ferroptosis is a novel programmed cell death form that relies on iron accumulation, which is marked by reduced or disappeared mitochondria cristae and lipid peroxidation. Unlike traditional apoptosis, it is considered that the measurement of lipid peroxidation and ACSL4 is essential to assess the occurrence of the ferroptosis process. The discovery of ferroptosis has led to a new understanding of tumorigenesis and cancer progression. In recent years, some researchers have found widespread inhibition of ferroptosis in the lung cancer microenvironment. Lung cancer cells can improve the induction threshold of ferroptosis by various measures, which can inhibit ferroptosis and facilitate the occurrence and progression of lung cancer. For example, Lai's study revealed that the serine threonine tyrosine kinase 1 in the lung cancer cell (SW900) could upregulate the level of GPX4 [6]. This results in the promotion of lung cancer cell proliferation and the inhibition of various ferroptosis-induced mitochondrial abnormalities, which caused the inhibition of ferroptosis in NSCLC. Alvarez's research demonstrated that the iron-sulfur cluster biosynthetic enzyme (NFS-1) was highly expressed in lung adenocarcinoma tissues [7]. Experiments indicated that NFS-1 could interfere with iron metabolism, reduce cell iron release, and significantly alleviated ferroptosis induced by hyperoxia. Besides, some other studies have shown that lung cancer tissue could inhibit ferroptosis by regulating lipid metabolism to inhibit lipid synthesis [8], compensate for the enzyme catalytic system's lack of GPX4 [9,10], and other mechanisms. In conclusion, inhibition of ferroptosis in lung cancer is a complex biological process and the specific

molecular mechanisms remain unclear. Several prior studies showed that prognostic models constructed based on several ferroptosis-related genes were possible to be used to predict the prognosis of patients with LUAD, and a potential correlation between ferroptosis and immune cell infiltration patterns was demonstrated in LUAD [11-13]. Based on the latest ferroptosis-related gene database, the present study aimed to verify the results of previous studies and attempted to explore new ferroptosis-related genes involved in LUAD and build a refined prognostic model for LUAD patients.

For our study, we first downloaded the RNA sequencing (RNA-Seq) and relevant clinical details from the cancer genome atlas (TCGA). Then, a signature for LUAD containing several ferroptosis-related genes was constructed on the basis of the TCGA cohort and evaluated in the gene expression omnibus (GEO) cohort. Finally, further functional enrichment analyses were performed to explore the probable mechanisms.

Material and Methods

Data collection

The RNA-Seq data of 535 LUAD patients and 59 adjacent non-cancerous tissues were obtained from TCGA (<https://portal.gdc.cancer.gov/>). The following keywords: 'bronchus and lung', 'TCGA', 'TCGA-LUAD', 'transcriptome profiling', 'Gene Expression Quantification', and 'HTSeq – FPKM' were applied. The clinical information of 522 LUAD patients was retrieved from TCGA by searching the following keywords: 'bronchus and lung', 'TCGA', 'TCGA-LUAD', 'clinical', and 'bcr xml'. Clinical data included age, gender, survival status, and TNM classification of LUAD patients. The present study was based on public data from the TCGA database. Therefore, the approval of a related ethical committee was not required for the present study. Additionally, the 260 ferroptosis-related genes were acquired from the FerrDb database (<http://www.zhounan.org/ferrdb/>). Ferroptosis-related genes are defined as genes closely involved in various physiological and biochemical processes of ferroptosis, such as oxidative stress, iron metabolism, lipid metabolism, etc., which serve a crucial role in the modulation of ferroptosis.

Prognostic Model Building and Validation

The differentially expressed genes (DEGs) were detected by the 'Limma' R package with the criteria of false discovery rate (FDR) <0.05. Ferroptosis-related DEGs were identified by taking the intersection of the DEGs in LUAD and ferroptosis-related genes screened out based on the univariate analysis of overall survival (OS). The *p*-values were adjusted using the Benjamini-Hochberg (BH) false discovery rate method. The STRING software (version 11.5) was used to create the interaction network for

the overlapping prognostic ferroptosis-related DEGs. Then, the ‘glmnet’ R package was applied to conduct the Lasso-penalized Cox regression to acquire the most powerful prognostic markers among the DEGs. The candidate DEGs with prognostic values were defined as independent variables in the regression analysis, whereas the response variables were the survival status of patients. After performing 10-fold cross-validations, the optimal penalty parameter (λ) was determined. The risk score was computed on the basis of a linear combination of the Cox regression coefficient for each prognostic gene with its corresponding expression value. Patients were dichotomized into the low- and high-risk groups depending on the median risk score. For the gene expression data in the signature, two-dimensionality reduction methods were conducted. Principal Components Analysis (PCA) was performed using the ‘prcomp’ function of the “stats” package in R/Bioconductor. T-distributed stochastic neighbor embedding (tsne) was conducted by using the ‘Rtsne’ package of R/Bioconductor. The optimal cut-off point of risk value was defined as the point with the most significant split (Log-Rank test) and determined by the ‘surv_cutpoint’ function in the survminer package. Besides, the ROC curve was constructed to investigate the predicting accuracy of the gene signature for LUAD using the ‘survivalROC’ R package.

Functional Enrichment Analysis

DEGs between low and high-risk groups were identified with a threshold of FDR <0.05 using the ‘Limma’ package for further functional analysis. GO and KEGG pathway enrichment were carried out with R/Bioconductor using the ‘clusterProfiler’ package with the criteria of $|\log_2FC| \geq 1$ and FDR <0.05. Adjusted *p*-values were calculated using the BH method. To evaluate the difference in the infiltration level of the immune response, the Single sample gene-set enrichment analysis (ssGSEA) was employed to estimate the relative immune cell infiltration levels using the ‘GSVA’ R package. The ssGSEA algorithm was performed to quantify the level of immune infiltration (calculated as ssGSEA score) based on the previously reported landmark genes and gene expression profiles.

Statistical Analysis

Statistical analyses were performed using the R programming language. The unpaired t-test was applied to determine the statistical differences between the tumor and adjacent normal tissues. The chi-squared statistic was employed to evaluate the differences in proportions. The differences in the ssGSEA scores were tested using the non-parametric Mann-Whitney test. For survival analysis, the Kaplan-Meier curve and Log-Rank test were applied to determine the OS between groups. Both uni- and multivariate analyses were performed to explore prognostic factors of OS. A two-tailed *p*-value of less than 0.05 was considered statistically significant.

Table 1. Clinical characteristics of the LUAD patients enrolled in the present study.

| Characteristics | TCGA-LUAD | GEO-LUAD |
|----------------------------|---------------|---------------|
| Sample size | 522 | 443 |
| Age (median, range) | 65.33 (33-88) | 64.42 (33-87) |
| Gender (%) | | |
| Female | 280 (53.6%) | 220 (49.7%) |
| Male | 242 (46.4%) | 223 (50.3%) |
| Stage (%) | | |
| I | 279 (53.4%) | 276 (62.3%) |
| II | 124 (23.8%) | 95 (21.4%) |
| III | 85 (16.3%) | 69 (15.6%) |
| IV | 26 (5.0%) | 0 |
| Unknown | 8 (1.5%) | 3 (0.7%) |
| TNM stage (%) | | |
| T | | |
| T1 | 172 (33.0%) | 150 (33.9%) |
| T2 | 281 (53.8%) | 251 (56.7%) |
| T3 | 47 (9.0%) | 28 (6.3%) |
| T4 | 19 (3.6%) | 12 (2.7%) |
| Tx | 3 (0.6%) | 2 (0.4%) |
| N | | |
| N0 | 335 (64.1%) | 299 (67.5%) |
| N1 | 98 (18.8%) | 88 (19.8%) |
| N2 | 75 (14.4%) | 53 (12.0%) |
| N3 | 2 (0.4) | 0 |
| Nx | 11 (2.1%) | 3 (0.7%) |
| Unknown | 1 (0.2) | 0 |
| M | | |
| M0 | 353 (67.6%) | NA |
| M1 | 25 (4.8%) | NA |
| Mx | 140 (26.8%) | NA |
| Unknown | 4 (0.8%) | NA |
| Survival status | | |
| OS days (median) | 902.5 | 1578 |

Results

Our study finally enrolled a total of 522 LUAD patients from the TCGA database and 443 LUAD patients from the GEO database. Key baseline demographic and clinical features of participants were displayed in **Table 1**. **Figure 1** showed the flow chart of the present study.

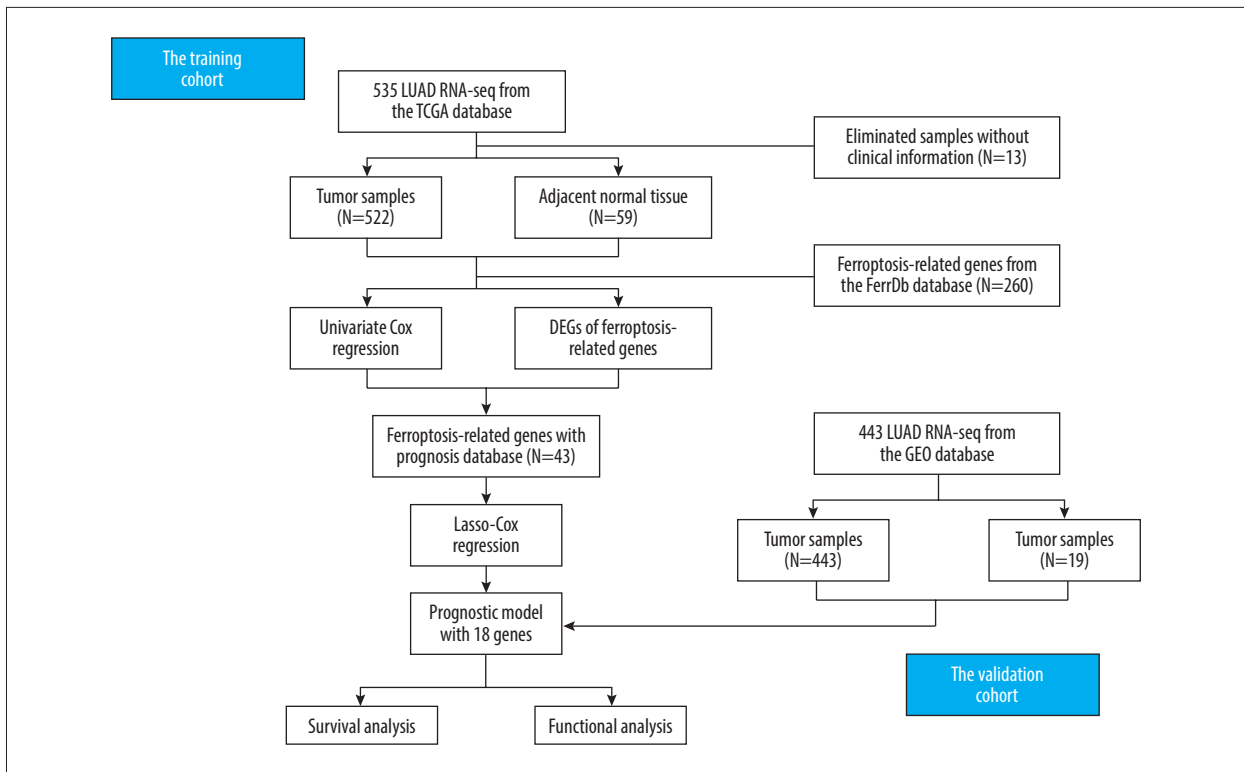


Figure 1. The flow diagram of the present study. (PowerPoint 2019, Microsoft Inc., Redmond, WA).

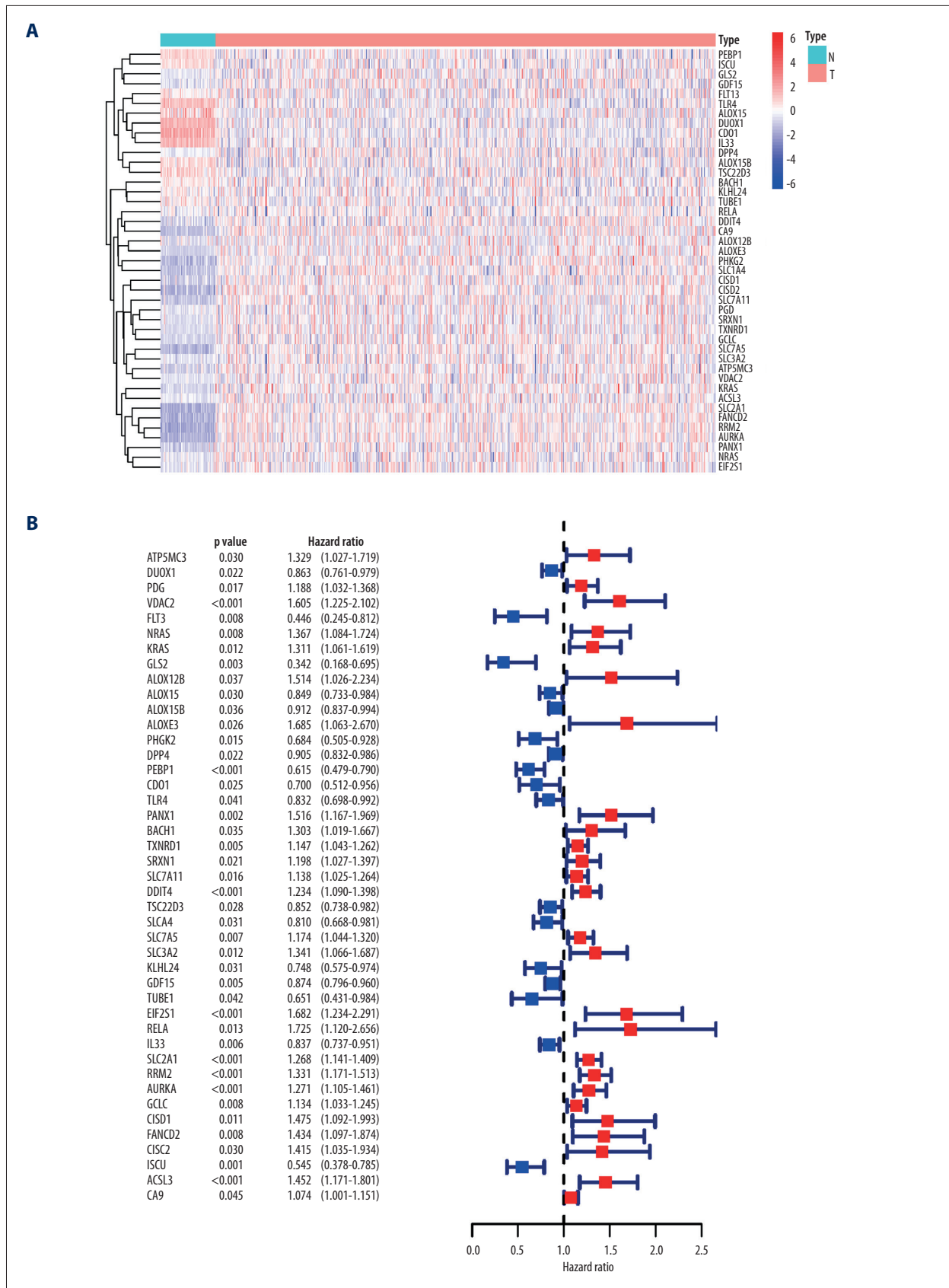
Identification of Prognostic DEGs in the TCGA Cohort

DEGs screening analysis revealed that the majority of the ferroptosis-related genes (181/260) were differentially expressed between LUAD tissues and corresponding adjacent non-cancerous tissues. The univariate analysis demonstrated that 43 of 181 ferroptosis-related genes were strongly linked to the OS of the LUAD patients (Supplementary Figure 1). These ferroptosis-related DEGs were altogether preserved with the standard of FDR<0.05 (Figure 2A, 2B). The constructed protein-protein interaction (PPI) network containing these DEGs revealed that KRAS, SLC3A2, and SLC2A1 were the hub genes (Figure 2C). The correlation network was presented in Figure 2D.

Generation of a Prognostic Signature Model

To further evaluate the prognostic effect of ferroptosis-related genes, 43 candidate genes were included in LASSO Cox regression analysis and 18 genes were filtered out according to the optimal value of λ (Supplementary Figure 2). The survival analysis demonstrated that 7 of high expression candidate genes (SLC2A1, RRM2, CISD1, CA9, DDIT4, EIF2S1, ACSL3) were associated with a bad prognosis, 6 of high expression candidate genes (PEBP1, GLS2, FLT3, SLC1A4, TLR4, TUBE1) were closely linked to a good survival outcome (all adjusted p<0.05, Supplementary Materials), while 5 of genes (RELA, PHKG2, KRAS, GDF15, ALOX12B) were not statistically

significant (adjusted p>0.05). The calculation method of risk score was listed as follows: $e^{(0.158 * \text{expression level of } RELA + 0.146 * \text{expression level of } ACSL3 + 0.116 * \text{expression level of } RRM2 + 0.113 * \text{expression level of } ALOX12B + 0.078 * \text{expression level of } CISD1 + 0.068 * \text{expression level of } EIF2S1 + 0.060 * \text{expression level of } DDIT4 + 0.013 * \text{expression level of } KRAS + 0.006 * \text{expression level of } CA9 + 0.002 * \text{expression level of } SLC2A1 - 0.09 * \text{expression level of } GDF15 - 0.067 * \text{expression level of } PHKG2 - 0.075 * \text{expression level of } SLC1A4 - 0.086 * \text{expression level of } TLR4 - 0.114 * \text{expression level of } FLT3 - 0.168 * \text{expression level of } TUBE1 - 0.210 * \text{expression level of } GLS2 - 0.214 * \text{expression level of } PEBP1)$. As the most commonly utilized index, the median score was selected as the cut-off value. A total of 250 patients were assigned to the low- and high-risk group on the basis of the median score (Supplementary Figure 3A). The high-risk group was found to be correlated with higher tumor grade and advanced TNM stage (Table 2). The PCA (Figure 3A) and tsne (Supplementary Figure 3B) analyses were performed for cluster analysis and visualization. Results demonstrated that patients were separated in 2 directions according to risk scores. Moreover, survival distribution demonstrated that patients with a high-risk score had greater mortality than patients with a low-risk score (Figure 3B). Similar results were also noticed in the survival curves (Figure 3C, P<0.001). The cut-off risk score for predicting survival was 0.127 (AUC 0.726, sensitivity 64%, specificity 69% for 1-year survival; AUC 0.726, sensitivity 61%, specificity 75% for 2-year survival; AUC 0.730, sensitivity 63%, specificity 72% for 3-year survival) (Figure 3D).



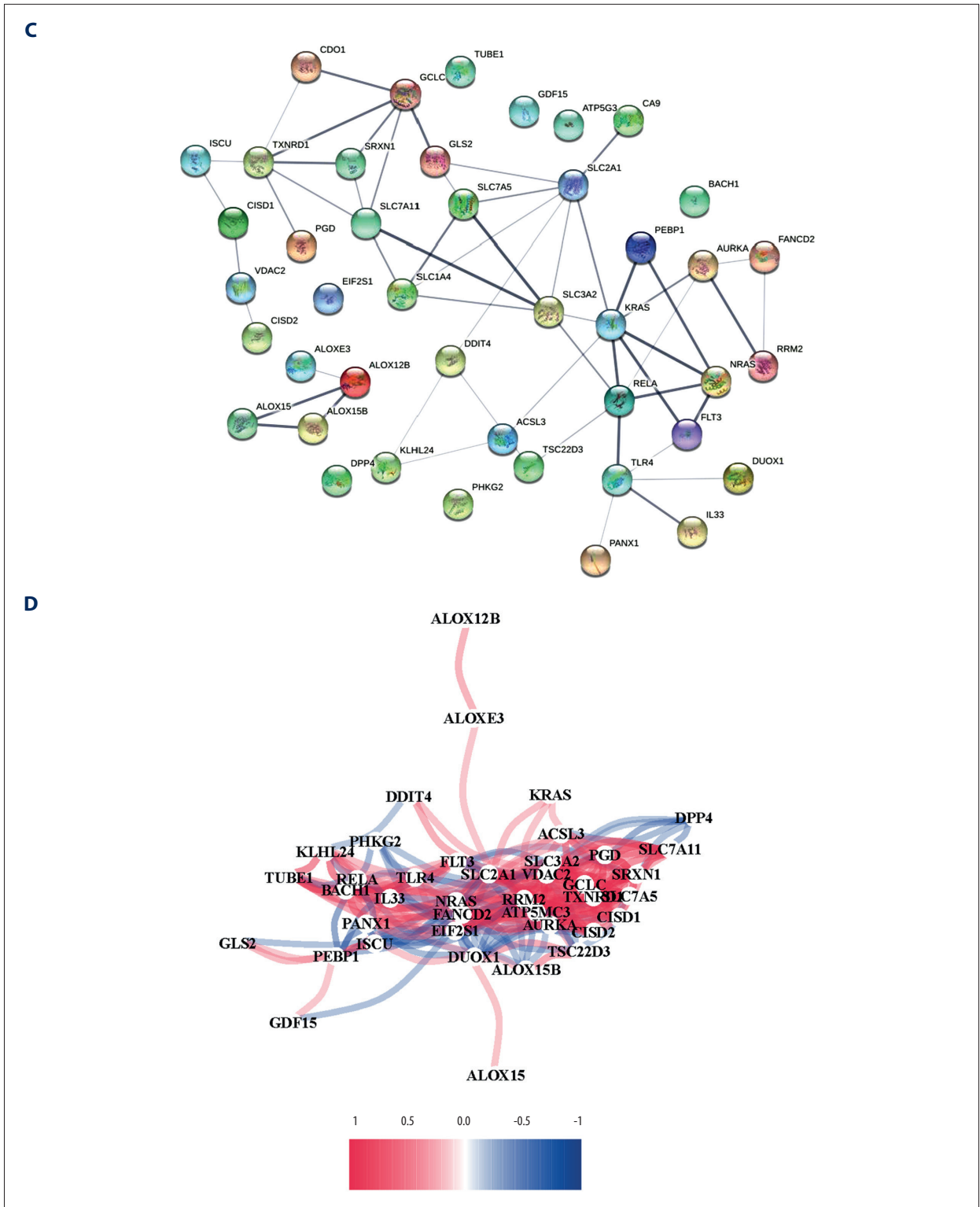


Figure 2. Identification of candidate genes related to ferroptosis in the TCGA cohort. **(A)** 43 DEGs were all upregulated in the LUAD tumor tissues. **(B)** The univariate analysis showed that 43 ferroptosis-related genes were correlated with the OS of LUAD patients. **(C)** The PPI network constructed by STRING displayed the interaction among the candidate genes. **(D)** The correlation network of candidate genes. Different colors represented different correlation coefficients. (R version 4.0.3, Ross Ihaka and Robert Gentleman, New Zealand; String version 11.5, <https://string-db.org/>).

Table 2. Baseline clinical features of the LUAD patients in both groups.

| Characteristics | TCGA-LUAD cohort | | | GEO-LUAD | | |
|----------------------|------------------|-------------|-----------------|------------|-------------|-----------------|
| | High risk | Low risk | <i>p</i> -value | High risk | Low risk | <i>p</i> -value |
| Gender (%) | | | | | | |
| Female | 123 (49.2%) | 147 (58.8%) | 0.031 | 7 (41.2%) | 212 (49.9%) | 0.481 |
| Male | 127 (50.8%) | 103 (41.2%) | | 10 (58.8%) | 213 (50.1%) | |
| Age (%) | | | | | | |
| ≤65 | 129 (51.6%) | 108 (43.2%) | 0.068 | 9 (52.9%) | 222 (52.2%) | 0.954 |
| >66 | 116 (46.4%) | 137 (54.8%) | | 8 (47.1%) | 203 (47.8%) | |
| Unknown | 5 (2.0%) | 5 (2.0%) | | 0 | 0 | |
| TNM stage (%) | | | | | | |
| I+II | 178 (71.2%) | 209 (83.6%) | 0.001 | 11 (64.7%) | 360 (84.7%) | 0.030 |
| III+IV | 68 (27.2%) | 37 (14.8%) | | 6 (35.3%) | 62 (14.6%) | |
| Unknown | 4 (1.6%) | 4 (1.6%) | | 0 | 3 (0.7%) | |

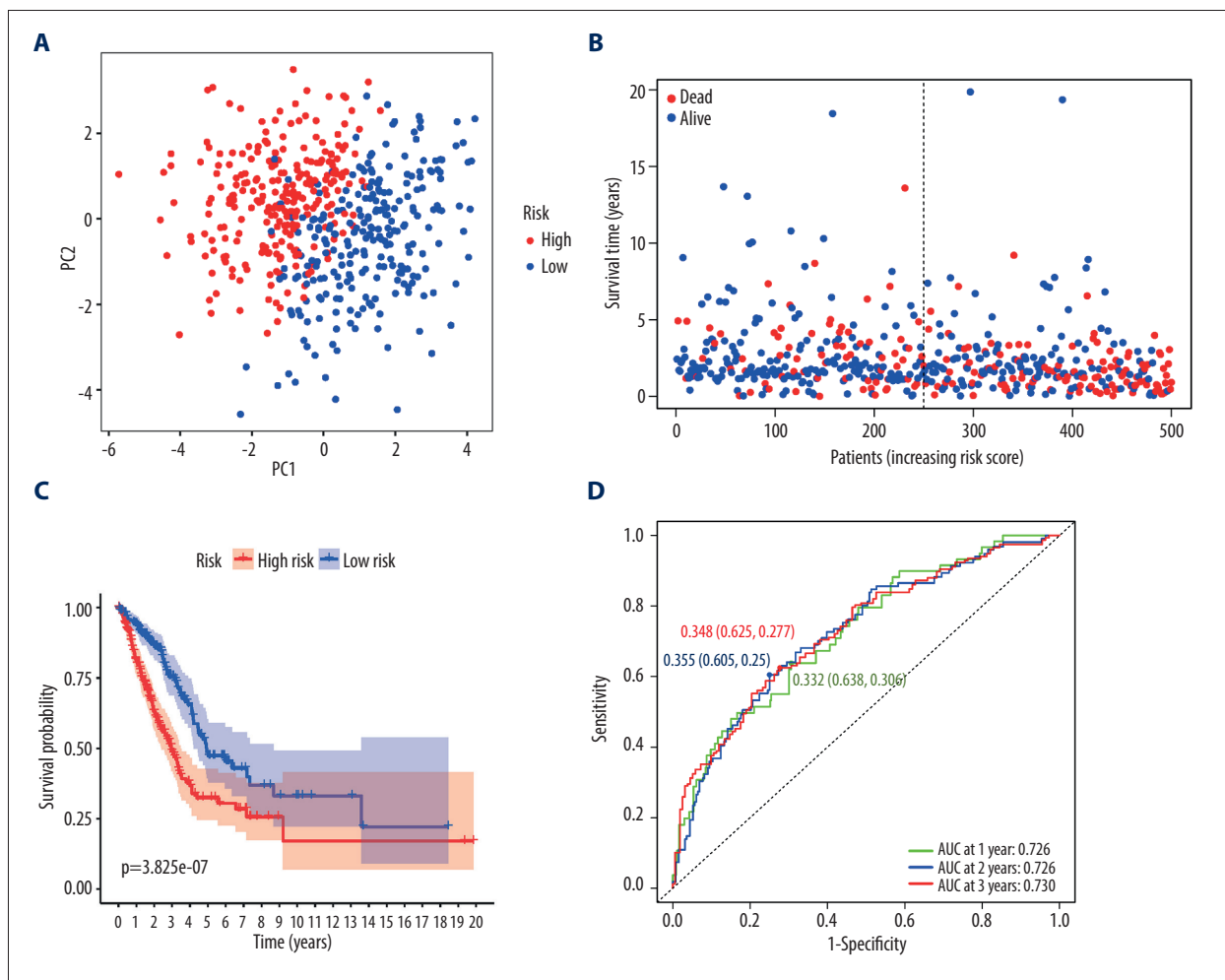


Figure 3. Generation of the prognostic model in the TCGA cohort. (A) PCA plot. (B) Survival of LUAD patients. (C) Kaplan-Meier OS curves for LUAD patients. (D) Time-dependent ROC curves. (R version 4.0.3, Ross Ihaka and Robert Gentleman, New Zealand).

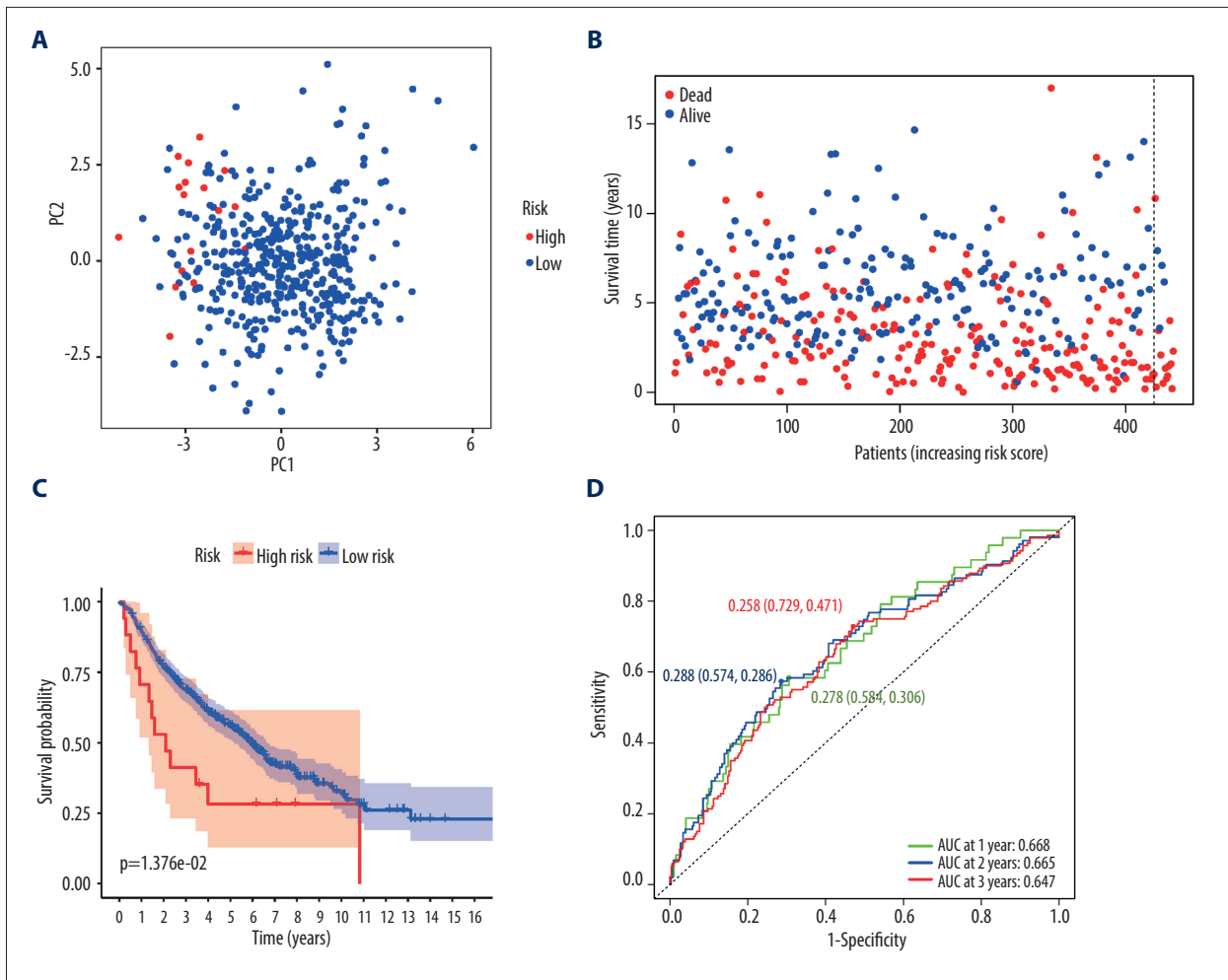


Figure 4. Validation of the prognostic model in the GEO cohort. (A) PCA plot. (B) Survival of LUAD patients. (C) Kaplan-Meier OS curves for LUAD patients. (D) Time-dependent ROC curves. (R version 4.0.3, Ross Ihaka and Robert Gentleman, New Zealand).

Validation of the Prognostic Model in the GEO Cohort

To further verify the robustness of the prediction model established from the training cohort, it was evaluated in the GSE68465 dataset. Patients were also dichotomized into 2 groups as previously described (Supplementary Figure 4A). Similar to the training group, the proportion of advanced LUAD patients (Stage III-IV) in the high-risk group was obviously higher (Table 2). Due to the uneven distribution of cases in the GEO cohort, PCA (Figure 4A) and tSNE (Supplementary Figure 4B) analysis could not identify the distribution difference. However, the distribution of the 2 groups could be roughly identified in a relatively discrete direction. The survival in the validation cohort was reduced with the increase in risk score (Figure 4B). Furthermore, the Kaplan-Meier survival curves revealed that the OS of the low-risk group had a significant survival advantage in comparison to the high-risk group (Figure 4C, $P < 0.05$). The cut-off values of risk score for predicting survival in the GEO cohort was -1.032 (AUC 0.668, sensitivity 58%, specificity

69% for 1-year survival; AUC 0.665, sensitivity 57%, specificity 71% for 2-year survival; AUC 0.647, sensitivity 73%, specificity 53% for 3-year survival) (Figure 4D).

Prognostic Value of the 18-Gene Signature

In order to investigate the prognostic value of novel signature for OS, both uni- and multivariate analyses of the signature-based risk score were carried out. In univariate analysis, the risk score was correlated with OS of LUAD patients (HR=5.590, 95% CI=3.647-8.567, $P < 0.001$). After correcting confounding factors in the multivariate analysis, the signature-based risk score was regarded as a valuable indicator for LUAD patients' OS (HR=5.167, 95% CI=3.306-8.075, $P < 0.001$) (Figure 5A). Similar results were also reached in the validation cohort. In the validation set, the univariate analysis revealed that a higher score was strongly linked with the worse OS of LUAD patients (HR= 1.482, 95% CI=1.235-1.778, $P < 0.001$). Multivariate analysis further demonstrated that the signature-based risk

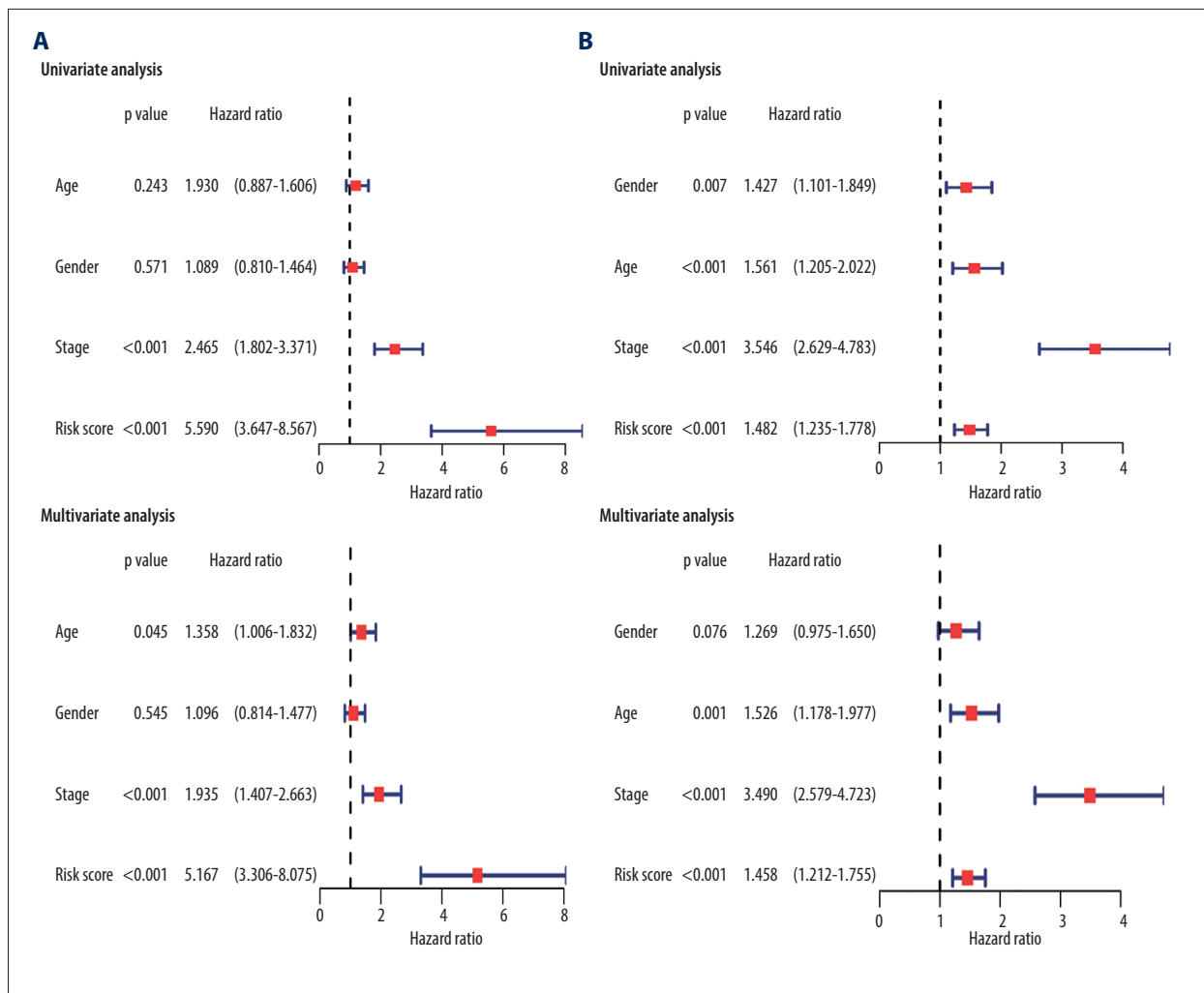


Figure 5. The uni- and multivariate analyses for OS in the TCGA cohort (A) and the GEO cohort (B). (R version 4.0.3, Ross Ihaka and Robert Gentleman, New Zealand).

score was the independent risk factor for patients with LUAD (HR=1.458, 95% CI=1.212-1.755, $P<0.001$) (Figure 5B).

Functional Enrichment Analysis of the DEGs

To explore the functions and biological pathways of the DEGs between the high-risk and low-risk groups, functional enrichment analyses were performed. The Gene Ontology (GO) provides a controlled vocabulary to elucidate a gene product's characteristics via its annotation. KEGG pathway enrichment provides data resources of known biological pathways to annotate a gene or a gene-set with their respective KEGG pathways.

As presented in Figure 6A, in terms of biological process (BP), the DEGs were enriched in the organelle fission, nuclear division, chromosome segregation, mitotic nuclear division, nuclear chromosome segregation. in terms of cellular component (CC), the DEGs were enriched in the spindle, microtubule,

condensed chromosome, chromosome, centromeric region, kinetochore. in terms of molecular function (MF), the DEGs were mainly enriched in the receptor-ligand activity, tubulin binding, microtubule-binding, peptidase regulator activity, endopeptidase inhibitor activity. Figure 6B showed signaling pathways were mostly enriched in the cell cycle, IL-17 signaling pathway, hematopoietic cell lineage, amoebiasis, complement and coagulation cascades.

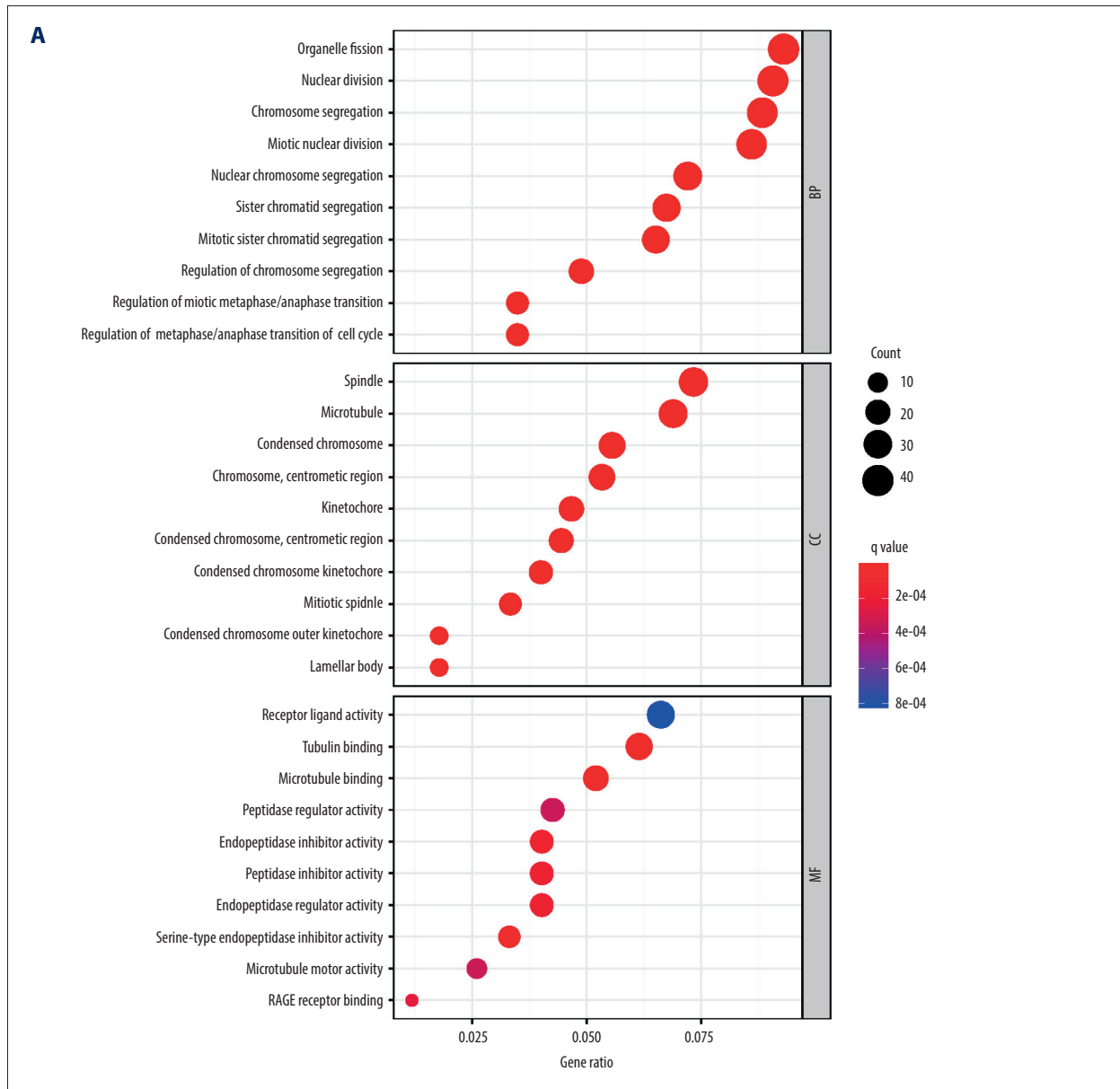
To further analyze the potential correlation between risk scores and immune response, the ssGSEA algorithm was employed to quantify enrichment levels of different immune components and related functions. Results showed that the scores of aDCs, B cells, DCs, iDCs, Macrophages, Mast cells, Neutrophils, pDCs, T helper cells, TIL, and Treg were significantly lower in the high-risk group than in the low-risk group (all adjusted $P<0.05$, Figure 7A). Besides, the scores of type APC co-stimulation, CCR, Check-point, HLA, T cell co-stimulation, Type II FN

Response were also significantly lower in low-risk LUAD patients when compared with high-risk LUAD patients. (All adjusted $P < 0.05$, **Figure 7B**).

Discussion

Lung cancer, especially LUAD, is a common malignancy with a severe incidence rate and mortality due to undetected pathogenesis. Currently, ferroptosis-related drugs are gaining increasing interest in cancer-related studies and are expected to provide a potential strategy for LUAD treatment [14,15]. Lung tissues are exposed to a higher oxygen concentration than other tissues. The huge oxidative pressure caused by a

special environment promotes lung cancer cells to suppress ferroptosis via various measures, thus leading to the progression of lung cancer. At present, the mechanisms of some therapeutic drugs have been revealed to be associated with ferroptosis in the existed classical treatment of lung cancer. For instance, research showed that cisplatin was an inducer of ferroptosis and apoptosis in A549 cells. The depletion of reduced GSH and the inactivation of GPX4 induced by cisplatin served a crucial role in the biological process. It was further found that combined treatment of cisplatin and Erastin (Class I FINS, ferroptosis-inducing agents) exerted strong synergistic effects on anti-tumor activity. Other drugs such as sulfasalazine [16] and sorafenib [17] have also been found to suppress lung cancer cell proliferation in vitro by reducing the levels of



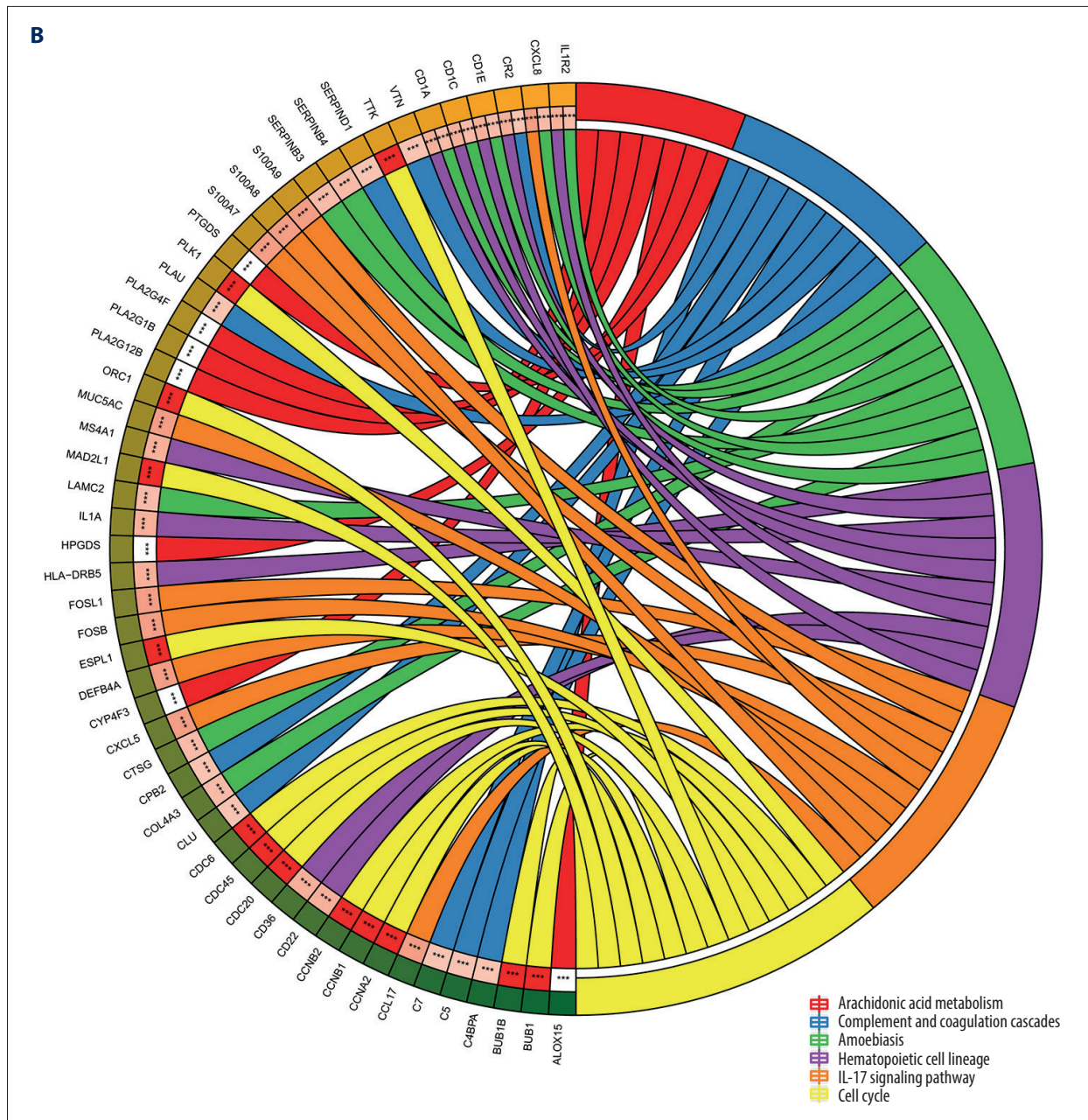


Figure 6. Functional enrichment analysis. (A) GO enrichment analysis of biological processes, cellular components, and molecular functions regarding the DEGs. (B) KEGG pathway analyses of DEGs. (R version 4.0.3, Ross Ihaka and Robert Gentleman, New Zealand).

GSH. Besides, some FINs could induce ferroptosis by directly reducing the activity of GPX4 and hence, exert anti-tumor effects in vitro. Therefore, studies on ferroptosis are opening up new opportunities for the development of anti-cancer therapies. Nonetheless, the correlation between ferroptosis-related genes and LUAD patients' outcomes needs to be clarified.

With deepening research, the model of multi-gene combination prediction has been gradually applied to the prognostic

analysis of tumor patients [18]. Classical LUAD biomarkers such as EGFR, ALK, ROS1, MET, etc., play a critical role in guiding molecular staging and treatment. Nevertheless, the value of individual biomarkers in prediction is limited due to the neglect of molecular interaction and simultaneous changes. It has been shown before that multi-gene assay could significantly improve the sensitivity, reproducibility, and robustness of tumor prognostic analysis [19] although it may need more medical expenses [20]. Anyhow, multi-gene association-based

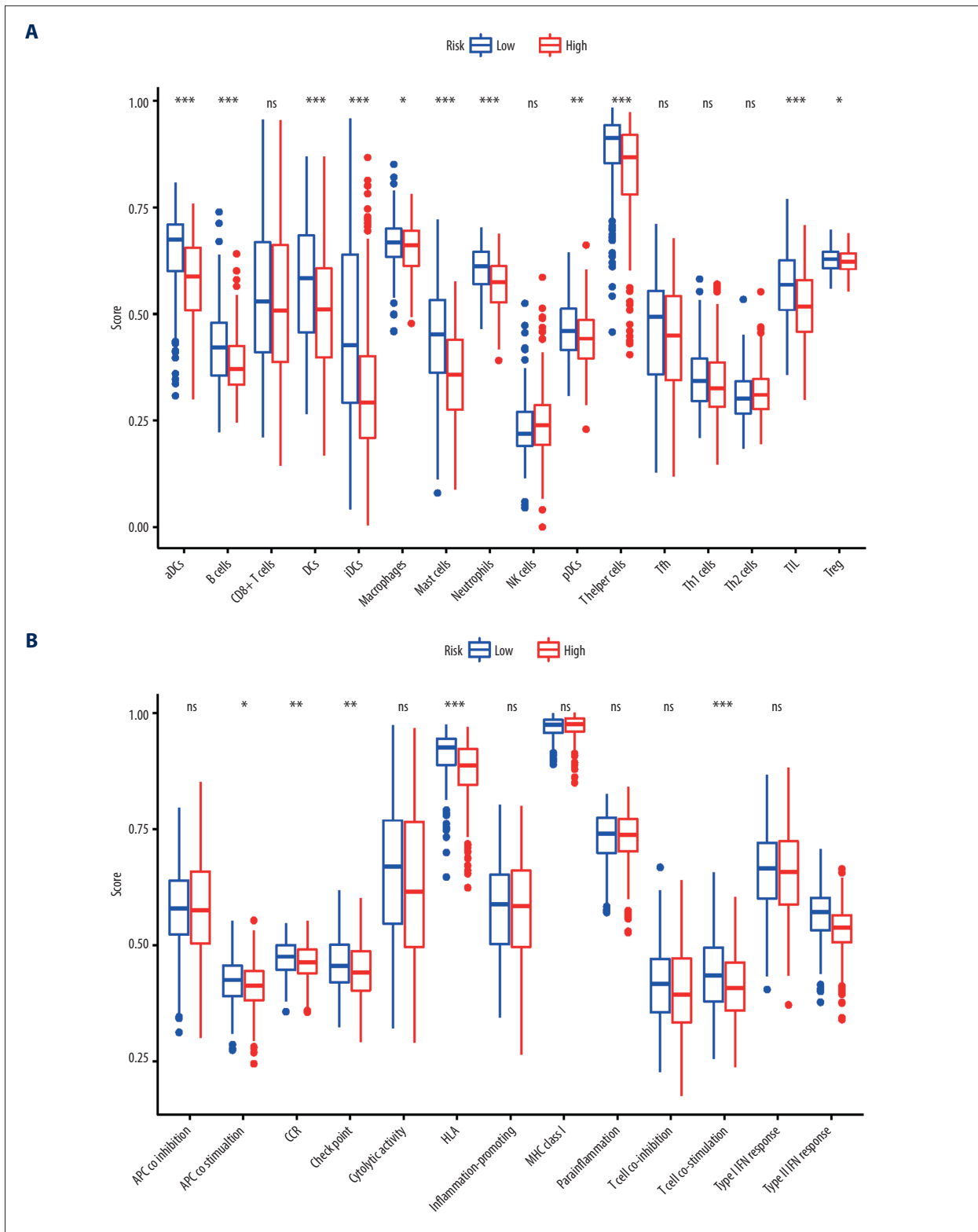


Figure 7. The immune cell subsets (A) and the immune-related functions (B) identified by the ssGSEA score-based method between high-risk and low-risk groups. Adjusted *p*-values: * *p*≤0.05, ** *p*≤0.01, *** *p*≤0.001. APC – antigen presenting cell; CCR – chemokine receptor; DCs – dendritic cells; HLA – human leukocyte antigen; IFN – interferon; MHC – major histocompatibility complex; TIL – tumor-infiltrating lymphocyte. (R version 4.0.3, Ross Ihaka and Robert Gentleman, New Zealand).

models may be the general trend in the development of prognostic analysis for tumor patients.

In the current work, we tried to build a feasible mathematical prognostic model for LUAD patients with ferroptosis-related genes. Results displayed that the majority of the ferroptosis-related genes (69.6%) were differentially expressed between tumors and adjacent non-cancerous tissues. Among them, 43 of 181 ferroptosis-related genes were strongly associated with the OS. These results confirmed the possibility to establish a ferroptosis-related genes-based signature for patients with LUAD. A prognostic model consisting of 18 ferroptosis-related genes was then constructed by multivariate Cox regression. Besides, to examine the robustness of the model, another independent dataset from GEO (GSE 68465) was introduced for validation.

For the prognostic signature, 7 high expression genes (*ACSL3*, *CA9*, *CISD1*, *DDIT4*, *EIF2S1*, *RRM*, *SCL2A1*) were correlated with poor prognosis, while 6 high expression genes (*FLT3*, *GLS2*, *PEBP1*, *SLC1A4*, *TLR4*, *TUB1*) were associated with better prognosis.

The function of ACSLs is to convert fatty acids into fatty acyl-CoA esters [21]. ACSL3 is mainly located in the endoplasmic reticulum and lipid droplets. Several pieces of research have demonstrated that overexpressed ACSL3 lead to worse clinical outcome in patients with NSCLC [22-24] and promoted a ferroptosis-resistant cell status [25]. Down-regulating ACSL3 causes the exhaustion of cellular ATP and cell death in lung cancer [24]. CA9 is a transmembrane enzyme participating in the metabolism of carbon dioxide to carbonic acid, thereby acidifying the extracellular milieu [26,27]. Several studies revealed that the high expression of CA9 was closely linked to the poor prognosis of lung cancer [26-29]. CA9 was also found to confer resistance to ferroptosis in malignant mesothelioma under hypoxia, which emerged as a promising therapeutic target for malignant mesothelioma. The CISD1 is an iron-containing protein located in the outer membranes of mitochondria. Studies showed that genetic inhibition of CISD1 could promote erastin-induced ferroptosis, which indicated the important role of CISD1 in protecting mitochondrial from injury in ferroptosis [30]. DDIT4 was noticed to be intimately linked to the poor prognosis of lung cancer [31,32]. However, the mechanism was mostly related to cell autophagy [33,34]. The relationship between DDIT4 and ferroptosis needs further study. EIF2S1, better known as eIF2 α , is a crucial member of eukaryotic initiation factors. A recent study showed that ferroptosis and apoptosis-related agents had interactions in the endoplasmic reticulum stress-mediated signaling pathway. Among them, the phosphorylation of eIF2 α played a key role [35,36]. Ribonucleotide reductase regulatory subunit M1 (RRM1) was reported to be linked to the poor prognosis of lung cancer

patients treated with gemcitabine. However, since few ferroptosis relevant studies on RRM and SCL2A1, the prognostic role of these genes still warrants to be further investigated [37].

FLT3 is a member of the type III receptor tyrosine kinase family and a ferroptosis promoter [38]. Research indicated that FLT3 inhibitors could prevent reactive oxygen species (ROS) generation and lipid peroxidation, which were the key mechanisms of ferroptosis [39]. Under the circumstances of glutaminase deficiency and the inhibition of glutamine decomposition, ROS and lipid oxidation accumulation of cells is inhibited, thus preventing the occurrence of ferroptosis. GLS2, namely glutaminase 2, is involved in the process of ferroptosis. Studies showed that GLS2 was the downstream target of the P53 gene, and overexpressing of GLS2 could promote P53-dependent ferroptosis [40]. Besides, a clinical metabolomic study indicated that EGFR mutated NSCLC was associated with high expression of GLS2 protein and mRNA [41]. PEBP1 is reported as an inhibitor of protein kinase cascades [42]. It is pivotal to complex with both 15LO1 and 15LO2, change the competence of their substrate to generate hydroperoxyl-PE, thus leading to ferroptosis [42-44]. A study showed that knocking down TLR4 could significantly inhibit ferroptosis-mediated cell death [45]. The prognostic values of SLC1A4 and TUB1 and their relationship with ferroptosis are less frequently reported, so further study is needed to confirm these findings.

Functional analyses demonstrated that DEGs were enriched in the immune response-related signaling pathway. For instance, Interleukin-17 (IL-17) was identified as having a vital role in the progression of lung cancer. A high level of IL-17 in the tumor microenvironment could recruit tumor-associated macrophages and induce the differentiation of macrophages to M2, thus promoting the proliferation and metastasis behavior [46]. IL-17 could also promote metastasis and invasion by activating epithelial-mesenchymal transformation via the NF- κ B/ZEB1 pathway [47]. A related clinical study indicated serum IL-17 level was a potential prognostic indicator for OS in LUAD patients [48-50]. It is therefore tempting to speculate that one of the mechanisms for ferroptosis influencing LUAD patients' outcomes may be correlated with affecting the IL-17 signaling pathway.

Additionally, remarkable differences were noticed in immune cell infiltration, especially in dendritic cells (DCs), tumor infiltration lymphocyte (TIL), mast cells, neutrophils, and Th cells. DCs is the key cell to stimulate the anti-tumor immune response in vivo and has the function of professional antigen presentation [51]. It could be divided into plasma DCs (pDCs) and myeloid DCs (mDCs) [52]. Lung cancer could lead to the differentiation disorder, abnormal maturation process, and aberrant phenotype of monocyte induced DCs, which become an important cause of tumor immune escape. The research suggested

that a high level of infiltrating mature DCs in the tumor environment is a positive prognostic indicator. TIL is another family of heterogeneous cells that play an important role in tumor-related immune responses. It consists of T lymphocyte, B lymphocyte, DC, and natural killer cells located in the tumor and its stroma. TIL is not only the reflection of the host's immune response to tumor cells but also is the basis of the body's recognition and removal of tumor cells. Studies have demonstrated that TIL cells were strongly linked to the positive prognosis of NSCLC, and could serve to assess the prognosis of lung cancer [53,54]. These are consistent with the results of our study. For immune function analysis, the low expression of APC co-stimulation, HLA, T cell co-stimulation, and Type II IFN response all indicated the low ability of antigen presentation and tumor immune escape inhibition, which was conducive to the tumor progression.

Taken together, in comparison with previous prognostic modeling researches [11-13], some common genes which have a significant influence on the prognosis of LUAD patients were further verified in our research, including ferroptosis driver genes (*FLT3*, *GLS2*, *PEBP1*) and ferroptosis suppress genes (*ACSL3*, *C1SD1*). Besides, some novel ferroptosis-related genes were proposed in the prognostic signature, such as *RELA*, *EIF2S1*, *TUBE1*, and *SCL2A1*.

There still exist several limitations in our study. Firstly, the prognostic signature was only proposed and verified by online gene databases in the present study. Further studies based on real-world data are needed to investigate the effectiveness of the

prediction model. Secondly, due to the limitation of the prognostic signature proposed only from the angle of ferroptosis, many other valuable predictive genes may be ignored. Thirdly, the role of these genes in modulating the progression of LUAD is awaiting further experimental validation.

Conclusions

Our study proposed an OS-related prediction model for LUAD patients with 18 ferroptosis-related genes. The model was then proved to be a powerful and valuable indicator for LUAD patients' OS in both training and validation cohorts. Further functional enrichment analysis revealed that these genes may be engaged in the modulation of anti-tumor immunity. However, the underlying mechanism remains to be further studied.

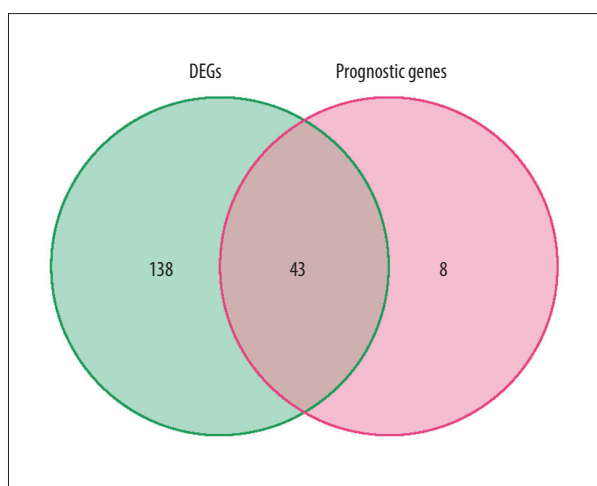
Data Availability

The research data that support the findings of the present study are available from the TCGA database (<https://portal.gdc.cancer.gov/>), the Gene Expression Omnibus database (<https://www.ncbi.nlm.nih.gov/gds/>) and FerrDb database (<http://www.zhounan.org/ferrdb/>).

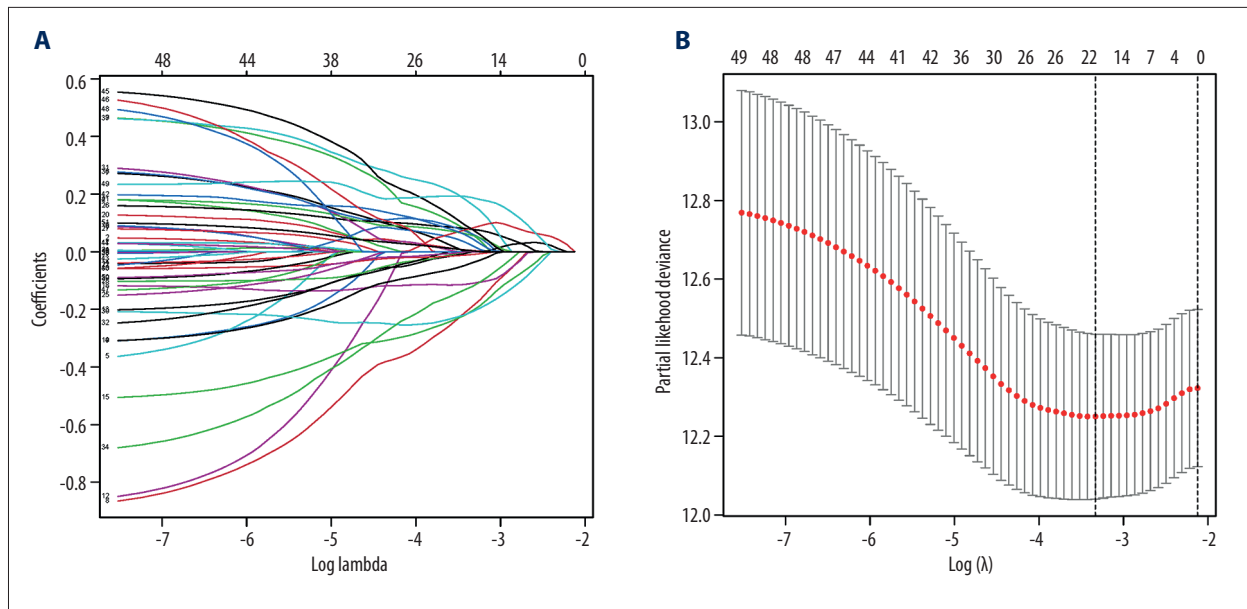
Declaration of Figures' Authenticity

All figures submitted have been created by the authors who confirm that the images are original with no duplication and have not been previously published in whole or in part

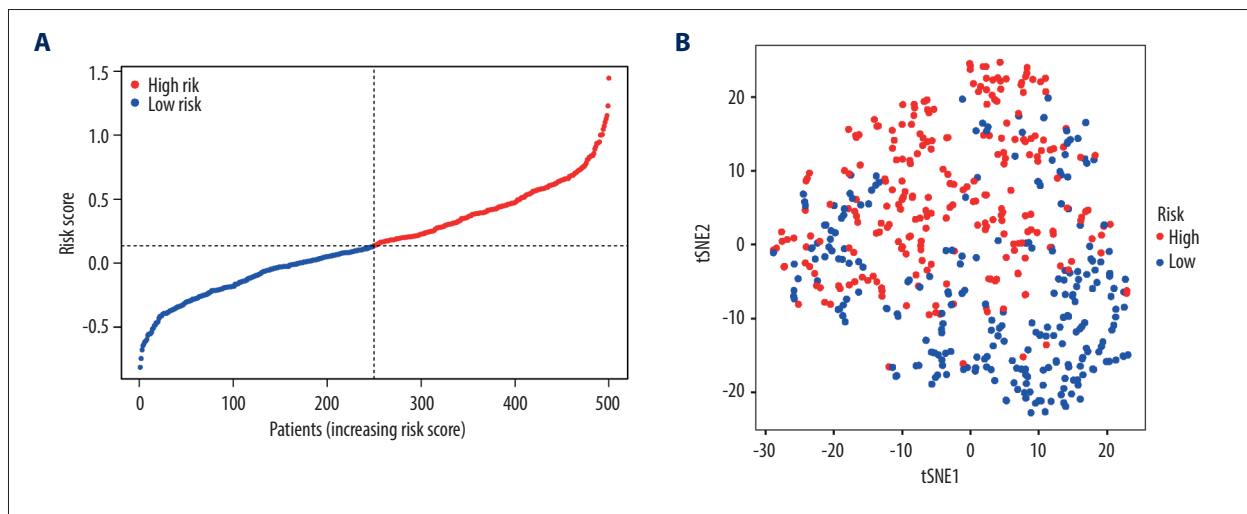
Supplementary Figures



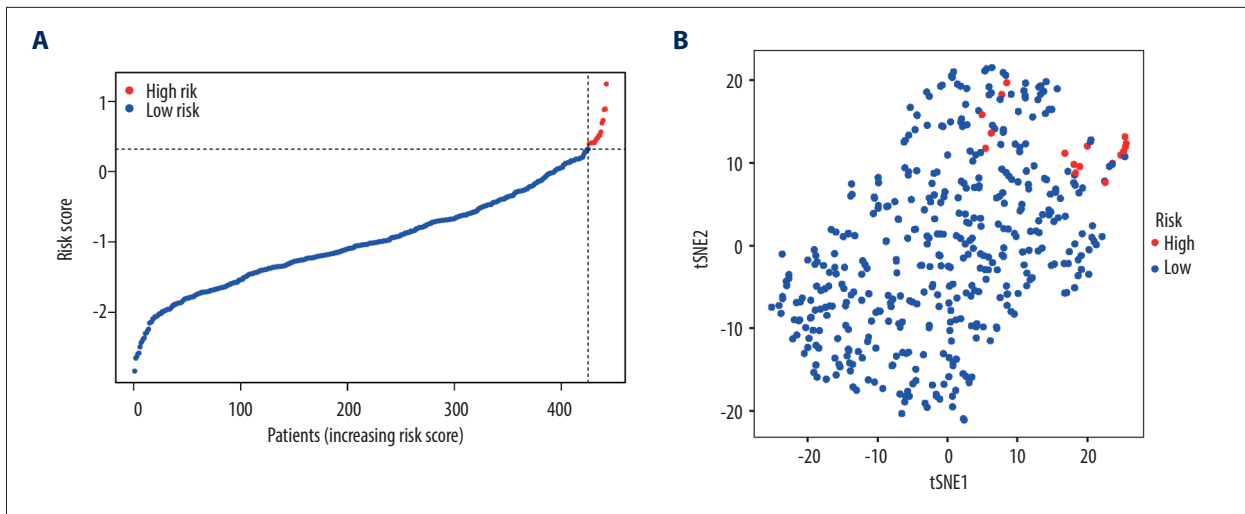
Supplementary Figure 1. Venn diagram of DEGs between the tumor tissues and the adjacent normal tissues. (R version 4.0.3, Ross Ihaka and Robert Gentleman, New Zealand).



Supplementary Figure 2. showed the construction of an 18-ferroptosis-related genes signature in the training cohort. **(A)** 43 candidate genes were included in the LASSO Cox regression analysis. **(B)** Selection of the λ in the LASSO model via 10-fold cross-validation. (R version 4.0.3, Ross Ihaka and Robert Gentleman, New Zealand).



Supplementary Figure 3. Generation of the prognostic signature model with 18 ferroptosis-related genes in the TCGA cohort. **(A)** Patients were assigned into the high and low-risk groups on the basis of the signature-based risk scores. **(B)** tSNE analysis. (R version 4.0.3, Ross Ihaka and Robert Gentleman, New Zealand).



Supplementary Figure 4. Validation of the prognostic signature model in the GEO cohort. (A) Signature-based scores were used to divide the patients into high and low-risk groups. (B) tSNE analysis. (R version 4.0.3, Ross Ihaka and Robert Gentleman, New Zealand).

Supplementary Materials

Supplementary Materials displayed the survival curves of 18-ferroptosis-related gene expression and prognosis in LUAD patients.

Supplementary materials available from the corresponding author on request.

References:

- Bray F, Ferlay J, Soerjomataram I, et al. Global cancer statistics 2018: GLOBOCAN estimates of incidence and mortality worldwide for 36 cancers in 185 countries. *Cancer J Clin*. 2018;68:394-424
- Feng RM, Zong YN, Cao SM, et al. Current cancer situation in China: Good or bad news from the 2018 Global Cancer Statistics? *Cancer Commun (Lond)*. 2019;39:22
- Cancer Genome Atlas Research Network. Comprehensive molecular profiling of lung adenocarcinoma. *Nature*. 2014;511:543-50
- Allemani C, Weir HK, Carreira H, et al. Global surveillance of cancer survival 1995-2009: Analysis of individual data for 25 676 887 patients from 279 population-based registries in 67 countries (CONCORD-2). *Lancet*. 2015;385:977-1010
- de Langen AJ, Smit EF. Therapeutic approach to treating patients with BRAF-mutant lung cancer: Latest evidence and clinical implications. *Ther Adv Med Oncol*. 2017;9:46-58
- Lai Y, Zhang Z, Li J, et al. STYK1/NOK correlates with ferroptosis in non-small cell lung carcinoma. *Biochem Biophys Res Commun*. 2019;519:659-66
- Alvarez SW, Sviderskiy VO, Terzi EM, et al. NFS1 undergoes positive selection in lung tumours and protects cells from ferroptosis. *Nature*. 2017;551:639-43
- Jiang Y, Mao C, Yang R, et al. EGLN1/c-Myc induced lymphoid-specific helicase inhibits ferroptosis through lipid metabolic gene expression changes. *Theranostics*. 2017;7:3293-305
- Bersuker K, Hendricks JM, Li Z, et al. The CoQ oxidoreductase FSP1 acts parallel to GPX4 to inhibit ferroptosis. *Nature*. 2019;575:688-92
- Doll S, Freitas FP, Shah R, et al. FSP1 is a glutathione-independent ferroptosis suppressor. *Nature*. 2019;575:693-98
- Chao M, Feng L, Huan L. Prognostic and immune implications of a novel ferroptosis-related ten-gene signature in lung adenocarcinoma. *Ann Transl Med*. 2021;9:1058
- Yuxuan W, Weikang C, Minqi Z, et al. Ferroptosis-related gene signature and patterns of immune infiltration predict the overall survival in patients with lung adenocarcinoma. *Front Mol Biosci*. 2021;8:692530
- Ziyuan R, Minghui H, Zhonglin W, et al. Ferroptosis-related genes in lung adenocarcinoma: Prognostic signature and immune, drug resistance, mutation analysis. *Front Genet*. 2021;12:672904
- Chen P, Wu Q, Feng J, et al. Erianin, a novel dibenzyl compound in Dendrobium extract, inhibits lung cancer cell growth and migration via calcium/calmodulin-dependent ferroptosis. *Signal Transduct Target Ther*. 2020;5:51
- Guo J, Xu B, Han Q, et al. Ferroptosis: A novel anti-tumor action for cisplatin. *Cancer Res Treat*. 2018;50:445-60
- Guan J, Lo M, Dockery P, et al. The xc- cystine/glutamate antiporter as a potential therapeutic target for small-cell lung cancer: Use of sulfasalazine. *Cancer Chemother Pharmacol*. 2009;64:463-72
- Lachaier E, Louandre C, Godin C, et al. Sorafenib induces ferroptosis in human cancer cell lines originating from different solid tumors. *Anticancer Res*. 2014;34:6417-22
- Kai Z, Zulei L, Hui T. Twenty-gene-based prognostic model predicts lung adenocarcinoma survival. *Onco Targets Ther*. 2018;11:3415-24
- Angelo G-P, Lucia T-F, Guillermo P-V, et al. Prediction of adjuvant chemotherapy response in triple negative breast cancer with discovery and targeted proteomics. *PLoS One*. 2017;12:e0178296
- Kamalakaran S, Varadan V, Janevski A, et al. Translating next generation sequencing to practice: opportunities and necessary steps. *Mol Oncol*. 2013;7:743-55
- Coleman R, Lewin T, Van Horn C, et al. Do long-chain acyl-CoA synthetases regulate fatty acid entry into synthetic versus degradative pathways? *J Nutr*. 2002;132:2123-26
- Chen WC, Wang CY, Hung YH, et al. Systematic analysis of gene expression alterations and clinical outcomes for long-chain acyl-coenzyme A synthetase family in cancer. *PLoS One*. 2016;11:e0155660
- Fernandez LP, Merino M, Colmenarejo G, et al. Metabolic enzyme ACSL3 is a prognostic biomarker and correlates with anticancer effectiveness of statins in non-small cell lung cancer. *Mol Oncol*. 2020;14:3135-52

24. Padanad MS, Konstantinidou G, Venkateswaran N, et al. Fatty acid oxidation mediated by Acyl-CoA synthetase long chain 3 is required for mutant KRAS lung tumorigenesis. *Cell Rep.* 2016;16:1614-28
25. Magtanong L, Ko PJ, To M, et al. Exogenous monounsaturated fatty acids promote a ferroptosis-resistant cell state. *Cell Chem Biol.* 2019;26:420-32.e9
26. Giatromanolaki A, Harris AL, Banham AH, et al. Carbonic anhydrase 9 (CA9) expression in non-small-cell lung cancer: Correlation with regulatory FOXP3+T-cell tumour stroma infiltration. *Br J Cancer.* 2020;122:1205-10
27. Giatromanolaki A, Koukourakis M, Sivridis E, et al. Expression of hypoxia-inducible carbonic anhydrase-9 relates to angiogenic pathways and independently to poor outcome in non-small cell lung cancer. *Cancer research.* 2001;61:7992-98
28. Cohen A, Khalil F, Welsh E, et al. Cell-surface marker discovery for lung cancer. *Oncotarget.* 2017;8:113373-402
29. Yu YY, Chiou HL, Tsao SM, et al. Association of Carbonic Anhydrase 9 polymorphism and the epithelial growth factor receptor mutations in lung adenocarcinoma patients. *Diagnostics (Basel).* 2020;10:266
30. Yuan H, Li X, Zhang X, et al. CISD1 inhibits ferroptosis by protection against mitochondrial lipid peroxidation. *Biochem Biophys Res Commun.* 2016;478:838-44
31. Liu C, Li Y, Wei M, et al. Identification of a novel glycolysis-related gene signature that can predict the survival of patients with lung adenocarcinoma. *Cell Cycle.* 2019;18:568-79
32. Pinto JA, Rolfo C, Raez LE, et al. In silico evaluation of DNA Damage Inducible Transcript 4 gene (DDIT4) as prognostic biomarker in several malignancies. *Sci Rep.* 2017;7:1526
33. Mu N, Lei Y, Wang Y, et al. Inhibition of SIRT1/2 upregulates HSPA5 acetylation and induces pro-survival autophagy via ATF4-DDIT4-mTORC1 axis in human lung cancer cells. *Apoptosis.* 2019;24:798-811
34. Xiao X, Wang G, Liu H. Study on the molecular mechanism of Rac3 on regulating autophagy in human lung cancer cells. *J BUON.* 2017;22:445-53
35. Lee YS, Lee DH, Choudry HA, et al. Ferroptosis-induced endoplasmic reticulum stress: Cross-talk between ferroptosis and apoptosis. *Mol Cancer Res.* 2018;16:1073-76
36. Szwed M, Sonstevold T, Overbye A, et al. Small variations in nanoparticle structure dictate differential cellular stress responses and mode of cell death. *Nanotoxicology.* 2019;13:761-82
37. Lee JJ, Maeng CH, Baek SK, et al. The immunohistochemical overexpression of ribonucleotide reductase regulatory subunit M1 (RRM1) protein is a predictor of shorter survival to gemcitabine-based chemotherapy in advanced non-small-cell lung cancer (NSCLC). *Lung Cancer.* 2010;70:205-10
38. Ampasavate C, Jutapakdee W, Phongpradist R, et al. FLT3, a prognostic biomarker for acute myeloid leukemia (AML): Quantitative monitoring with a simple anti-FLT3 interaction and flow cytometric method. *J Clin Lab Anal.* 2019;33:e22859
39. Kang Y, Tiziani S, Park G, et al. Cellular protection using Flt3 and PI3Kalpha inhibitors demonstrates multiple mechanisms of oxidative glutamate toxicity. *Nat Commun.* 2014;5:3672
40. Kang R, Kroemer G, Tang D. The tumor suppressor protein p53 and the ferroptosis network. *Free Radic Biol Med.* 2019;133:162-68
41. Meijer TWH, Looijen-Salamon MG, Lok J, et al. Glucose and glutamine metabolism in relation to mutational status in NSCLC histological subtypes. *Thorac Cancer.* 2019;10:2289-99
42. Wenzel SE, Tyurina YY, Zhao J, et al. PEBP1 wards ferroptosis by enabling lipoxygenase generation of lipid death signals. *Cell.* 2017;171:628-41.e26
43. Koutsakis G, Nellis GF, Ghandhi JB. Surface temperature of a multi-layer thermal barrier coated wall subject to an unsteady heat flux. *Int J Heat Mass Transf.* 2020;155
44. Zhao J, Dar HH, Deng Y, et al. PEBP1 acts as a rheostat between prosurvival autophagy and ferroptotic death in asthmatic epithelial cells. *Proc Natl Acad Sci USA.* 2020;117:14376-85
45. Chen X, Xu S, Zhao C, et al. Role of TLR4/NADPH oxidase 4 pathway in promoting cell death through autophagy and ferroptosis during heart failure. *Biochem Biophys Res Commun.* 2019;516:37-43
46. Liu L, Ge D, Ma L, et al. Interleukin-17 and prostaglandin E2 are involved in formation of an M2 macrophage-dominant microenvironment in lung cancer. *J Thorac Oncol.* 2012;7:1091-100
47. Gu K, Li M, Shen J, et al. Interleukin-17-induced EMT promotes lung cancer cell migration and invasion via NF- κ B/ZEB1 signal pathway. *Am J Cancer Res.* 2015;5:1169-79
48. Pan B, Che D, Cao J, et al. Interleukin-17 levels correlate with poor prognosis and vascular endothelial growth factor concentration in the serum of patients with non-small cell lung cancer. *Biomarkers.* 2015;20:232-39
49. Lin Q, Xue L, Tian T, et al. Prognostic value of serum IL-17 and VEGF levels in small cell lung cancer. *Int J Biol Markers.* 2015;30:e359-63
50. Xu C, Hao K, Yu L, et al. Serum interleukin-17 as a diagnostic and prognostic marker for non-small cell lung cancer. *Biomarkers.* 2014;19:287-90
51. Steinman RM. Decisions about dendritic cells: Past, present, and future. *Annu Rev Immunol.* 2012;30:1-22
52. Merad M, Sathe P, Helft J, et al. The dendritic cell lineage: Ontogeny and function of dendritic cells and their subsets in the steady state and the inflamed setting. *Annu Rev Immunol.* 2013;31:563-604
53. Hendry S, Salgado R, Gevaert T, et al. Assessing tumor-infiltrating lymphocytes in solid tumors: A Practical review for pathologists and proposal for a standardized method from the International Immuno-Oncology Biomarkers Working Group: Part 2: TILs in melanoma, gastrointestinal tract carcinomas, non-small cell lung carcinoma and mesothelioma, endometrial and ovarian carcinomas, squamous cell carcinoma of the head and neck, genitourinary carcinomas, and primary brain tumors. *Adv Anat Pathol.* 2017;24:311-35
54. Al-Shibli KI, Donnem T, Al-Saad S, et al. Prognostic effect of epithelial and stromal lymphocyte infiltration in non-small cell lung cancer. *Clin Cancer Res.* 2008;14:5220-27